SUPPLEMENTARY MATERIAL: Seasonal to decadal dynamics of supraglacial lakes on debris-covered glaciers

Lucas Zeller[1], Daniel McGrath[1], Scott W. McCoy[2], and Jonathan Jacquet[2]

[1]Department of Geosciences, Colorado State University, Fort Collins, CO 80523, USA
[2]3Department of Geological Sciences and Engineering, University of Nevada, Reno, NV 89557, USA

Correspondence: Lucas Zeller (Lucas.Zeller@colostate.edu)

1 PlanetScope Shadow Masking

A novel texture-based approach was developed to identify and mask out terrain shadowing in PlanetScope images. Shadows were identified on the glacier surface as large, continuous areas that were dark and had little spatial variation in brightness. These areas were identified using a multi-step process. First, areas of very high confidence shadow (shadow "seeds") were identified. These were identified if it met the following criteria:

1. The average surface brightness in visible bands was less than 1000 (using the image digital numbers).
2. At least 75% of on-glacier pixels within 99 meters had surface brightness less than 1000
3. The standard deviation of surface brightness of pixels within 99 meters was less than 50

These areas of shadow seeds were then iteratively expanded to include the continuous regions surrounding them with pixel brightness below the 1000 DN threshold in visible bands, with small voids and gaps filled.

2 Landsat Glacier Ice Masking

Continuously exposed areas of glacier ice in Landsat images were identified using thresholding on the normalized difference snow index (NDSI) and blue band surface reflectance. As a first step, areas of snow/ice were identified as pixels with an NDSI value greater than 0.2 and blue reflectance greater than 0.35. In order to avoid mis-classifying temporary snow cover, ice cliffs, or frozen lake surfaces as glacier ice we then applied a temporal smoothing to these products. For each Landsat image, pixels were given a final classification of glacier ice if that pixel was identified as ice using the aforementioned thresholds in greater than 60% of all Landsat images captured within the surrounding four years (two years before and after). These final glacier ice extents were then excluded from being classified as water.

Table S1. Number of observations and physical characteristics of each of the eight glaciers investigated. Note that all columns, other than "Total Glacier Size" refer to only the areas of investigation (AOI) used in this study. Ice flow velocities are given by the mean plus/minus one standard deviation. Note that Imja and Lhotse Shar (*) are considered a single glacier in RGI 6.0 (RGI Consortium, 2017). Debris thicknesses were taken from Rounce et al. (2021), and flow velocities were taken from NASA ITS_LIVE velocity mosaics (Gardner et al., 2022)

Glacier	Debris-covered Area (km^2, within AOI)	Total Glacier Size (km^2, RGI 6.0)	Glacier Length (km, within AOI)	Average debris thickness (m, within AOI)	Flow velocity (m yr^{-1}, within AOI)
Ama Dablam	2.23	4.82	3.87	1.04	0.76 $\pm$0.96
Ambulapcha	0.91	1.92	1.72	0.51	0.82 $\pm$0.40
Imja	1.01	14.27*	1.59	0.20	1.38 $\pm$1.39
Khumbu	5.74	19.10	8.09	0.82	1.53 $\pm$2.97
Lhotse	5.21	6.83	5.81	0.13	3.30 $\pm$6.06
Lhotse Nup	1.60	2.84	3.54	0.44	1.02 $\pm$1.25
Lhotse Shar	3.21	14.27*	3.41	0.43	3.35 $\pm$4.40
Nuptse	2.77	3.69	5.20	0.33	3.05 $\pm$4.07

Table S2. Number of images for each glacier from each source, after manual filtering of images with cloud cover, snow cover, or poor image quality.

Glacier	Planet	Landsat 5	Landsat 7	Landsat 8	Landsat 9	Sentinel-2
Pre-filtering		324	394	204	20	288
Ama Dablam	495	148	174	91	6	83
Ambulapcha	467	139	169	98	10	95
Imja	411	167	190	113	12	111
Khumbu	306	174	0	104	9	108
Lhotse	371	153	181	89	10	101
Lhotse Nup	468	162	209	97	12	112
Lhotse Shar	338	160	183	96	13	116
Nuptse	422	160	173	92	9	115

Table S3. Error statistics for SGL identification on each glacier. Comparing Planet-derived lake area to Landsat Sentinel-2 derived area. Presented as the mean difference in SGL area across all coincident imagery for each glacier (in m^2), and then normalized by debris-covered area (as %)

	Landsat 8 & 9		Sentinel-2	
Glacier	MAE (m^2 and %)	Bias (m^2 and %)	MAE (m^2 and %)	Bias (m^2 and %)
Ama Dablam	6231 (0.279%)	3557 (0.158%)	5181 (0.232%)	1520 (0.068%)
Ambulapcha	4213 (0.458%)	3969 (0.431%)	3906 (0.427%)	3377 (0.369%)
Imja	1212 (0.120%)	988 (0.098%)	705 (0.070%)	589 (0.059%)
Khumbu	56465 (0.987%)	52140 (0.912%)	59841 (1.043%)	59841 (1.043%)
Lhotse	29923 (0.574%)	25956 (0.498%)	38414 (0.546%)	12240 (0.236%)
Lhotse Nup	6107 (0.381%)	6085 (0.380%)	3549 (0.221%)	1646 (0.103%)
Lhotse Shar	24582 (0.766%)	24582 (0.766%)	19489 (0.608%)	17527 (0.546%)
Nuptse	18310 (0.663%)	18068 (0.654%)	12981 (0.469%)	12699 (0.459%)
Overall	14542 (0.486%)	13322 (0.445%)	14895 (0.426%)	12182 (0.336%)

Table S4. Long-term trends in SGL area on each glacier, as seen in Landsat-derived SGL products. Trends are presented as the lake area change per year from linear regression analysis of the entire timeframe (1988-2022) as well as only for the 2013-2022 period. Results are further broken down by glacier-wide lake area trends near-terminus (lower 50% by distance from terminus) trends. P-values are provided for each.

Glacier	Full Glacier 1988–2022 $m^2\ yr^{-1}$ (P-value)	Full Glacier 2013–2022 $m^2\ yr^{-1}$ (P-value)	Terminus only 1988–2022 $m^2\ yr^{-1}$ (P-value)	Terminus only 2013–2022 $m^2\ yr^{-1}$ (P-value)
Ama Dablam	156 (0.101)	-1009 (0.064)	47 (0.340)	-919 (0.029)
Ambulapcha	239 (0.000)	794 (0.071)	178 (0.000)	1034 (0.002)
Imja	-46 (0.073)	0 (1.0)	-41 (0.026)	0 (1.0)
Khumbu	2465 (0.000)	12821 (0.000)	2488 (0.000)	13497 (0.000)
Lhotse	754 (0.033)	3281 (0.118)	414 (0.074)	4876 (0.004)
Lhotse Nup	-27 (0.551)	-27 (0.895)	5.67 (0.706)	-35.45 (0.797)
Lhotse Shar	-743 (0.010)	-1047 (0.271)	-102 (0.148)	11 (0.970)
Nuptse	112 (0.213)	431 (0.361)	246 (0.000)	821 (0.165)

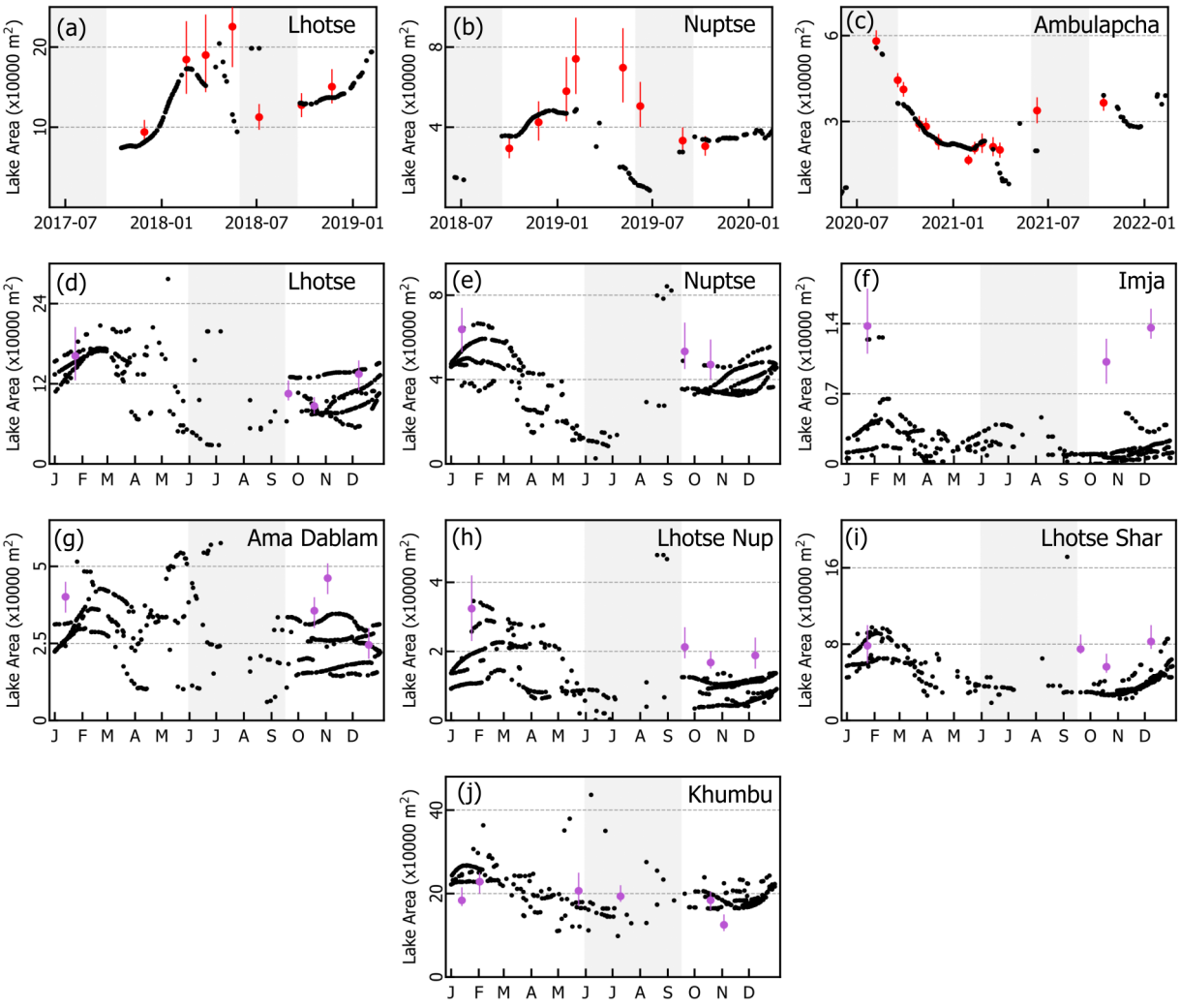

Figure S1. a-c) A comparison of automated lake areas (black dots) to the manually-delineated validation images on Lhotse, Nuptse, and Ambulapcha Glaciers (red). d-j) Comparison between automated lake areas and results from Watson et al. (2016, purple). Comparisons with Watson et al. are presented with results plotted by day of year (tick labels indicating the beginning of each month), as there was no temporal overlap between our observations and theirs. Grey shaded areas indicate monsoon months. Red and purple bars indicate error estimates from a ± 1 pixel buffering.

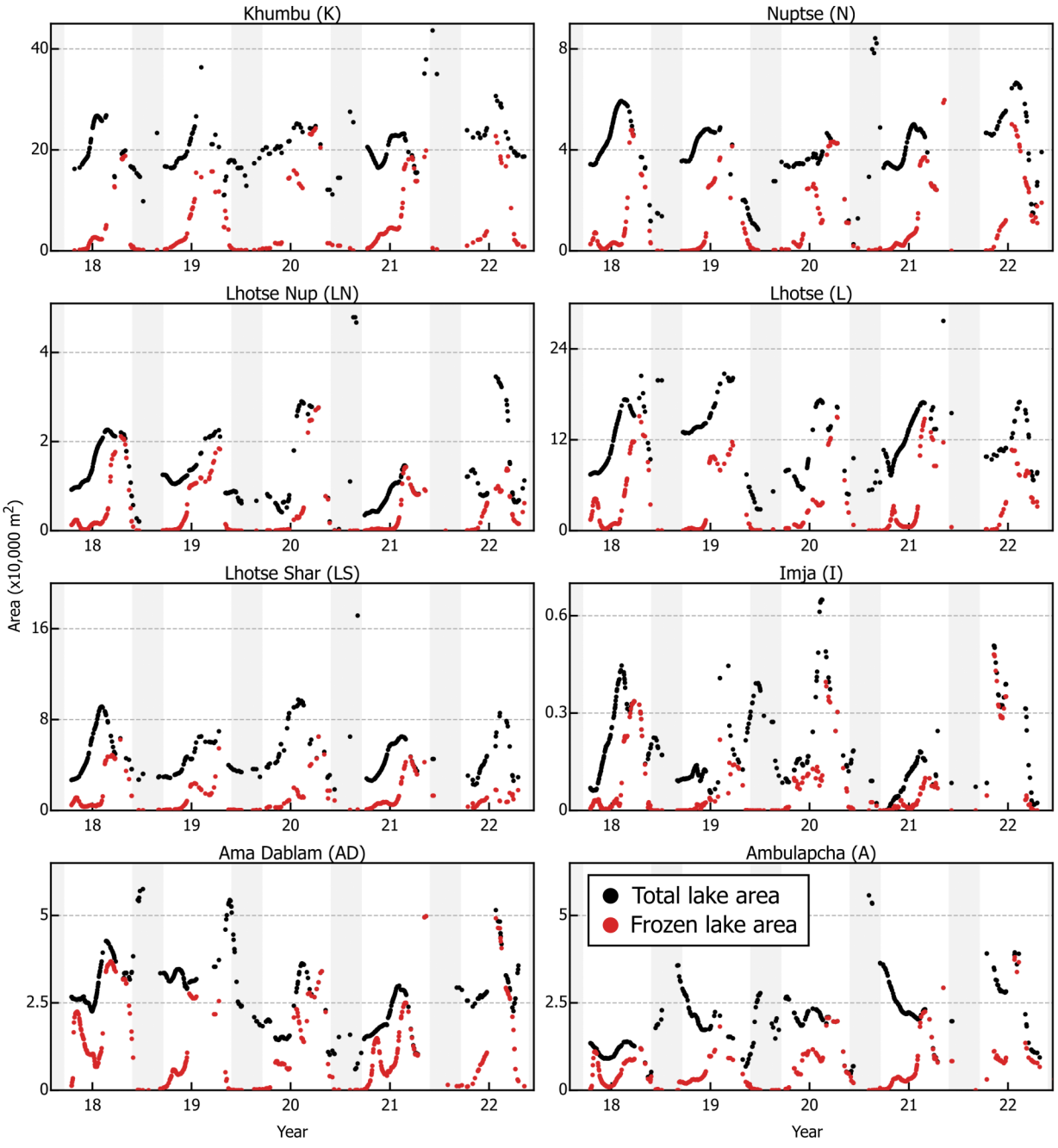

Figure S2. Comparison of the timeseries of total lake area (black points) and the total area of lake surface which are frozen (red points) for each glacier across the five-year study period.

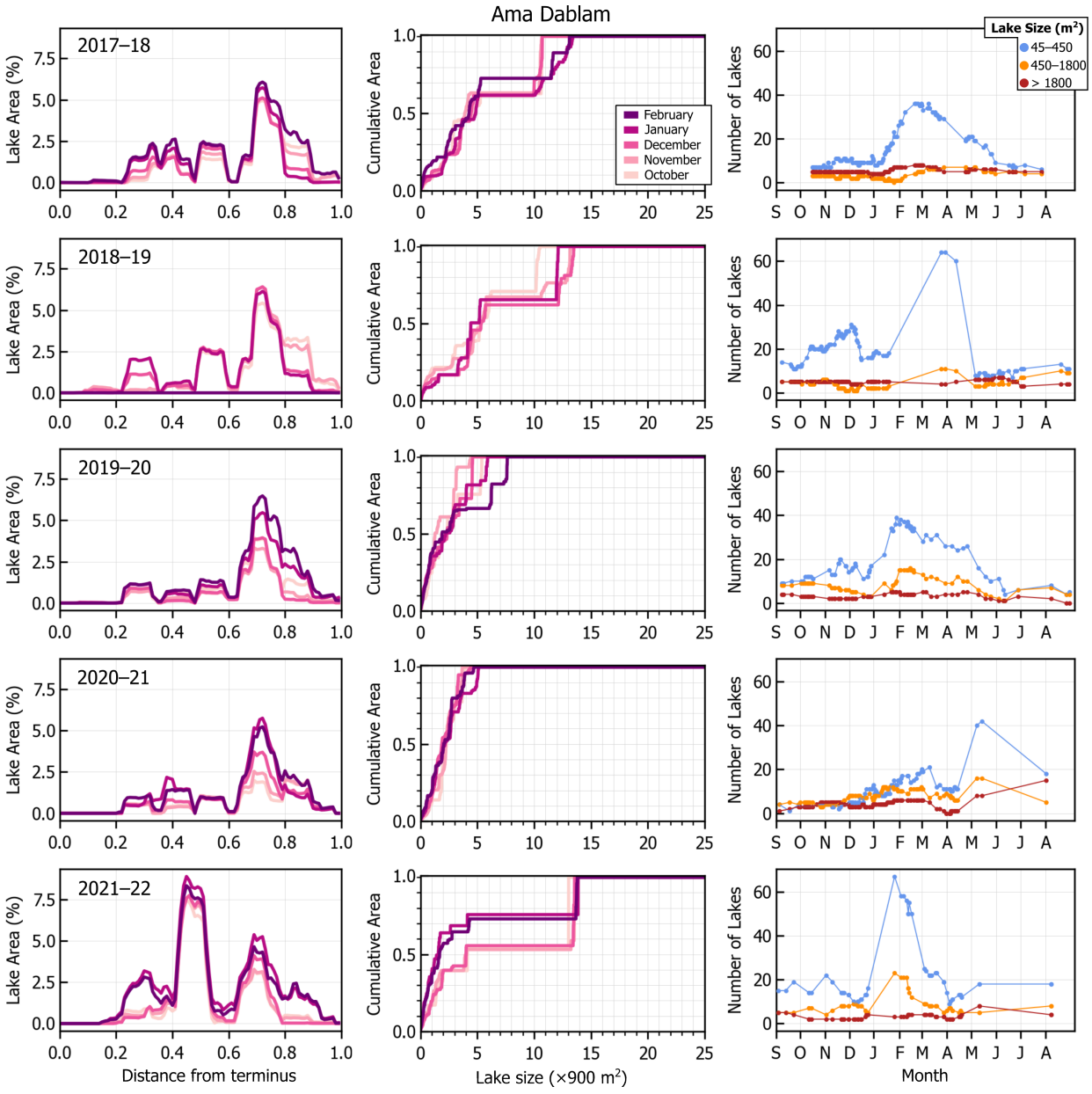

Figure S3. Seasonality in lake area and count on Ama Dablam Glacier, presented identically as Figure 10.

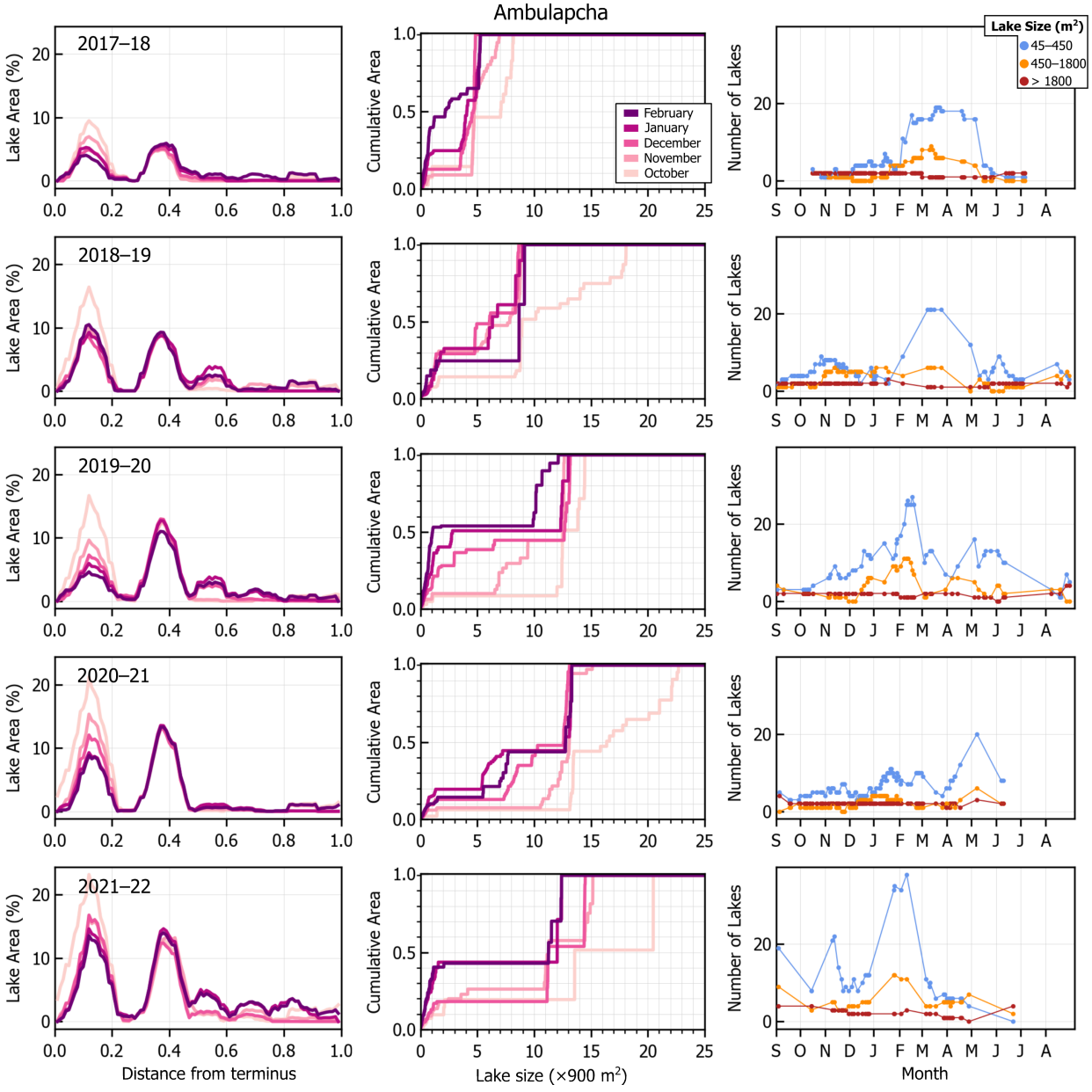

Figure S4. Seasonality in lake area and count on Ambulapcha Glacier, presented identically as Figure 10.

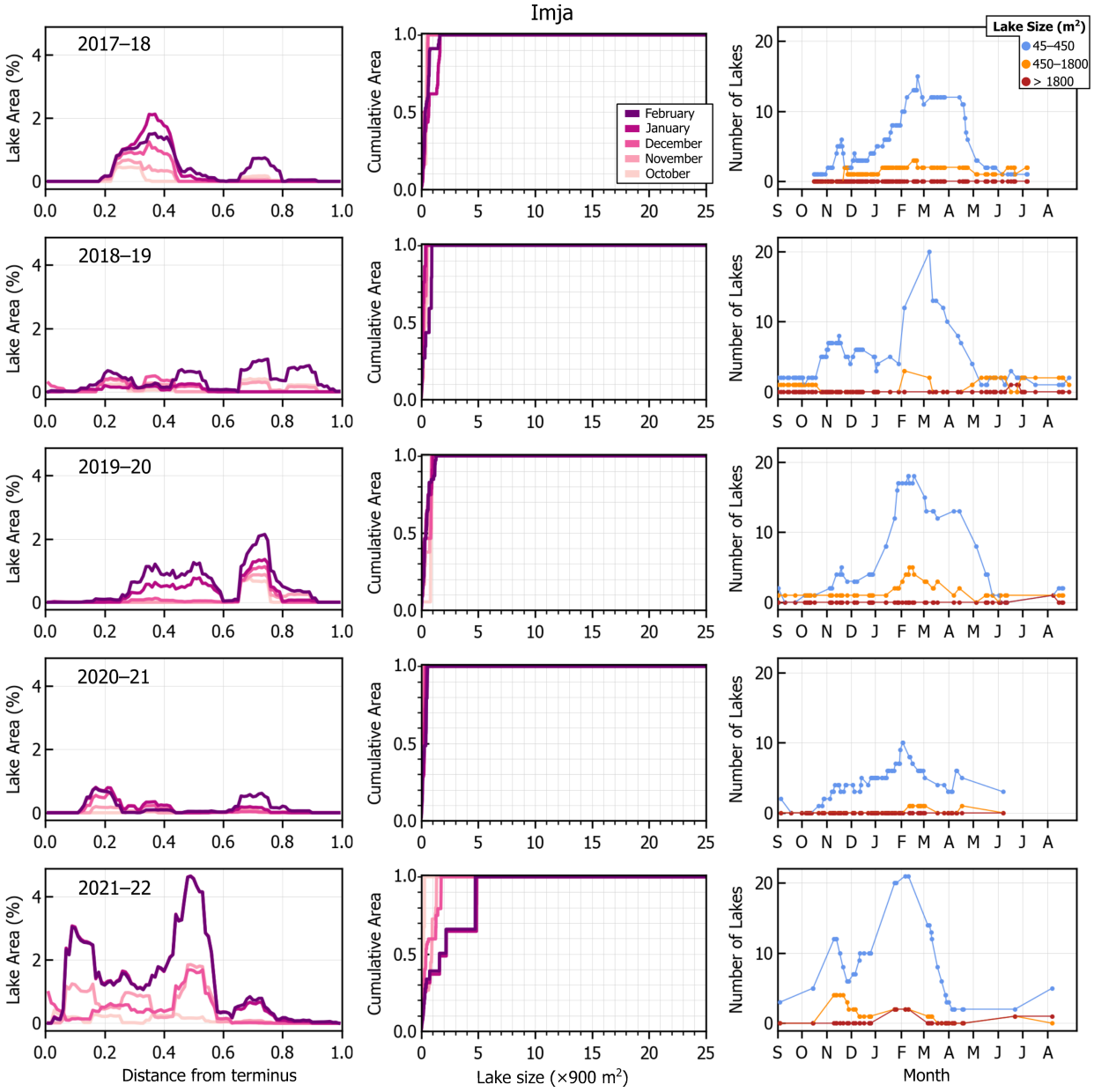

Figure S5. Seasonality in lake area and count on Imja Glacier, presented identically as Figure 10.

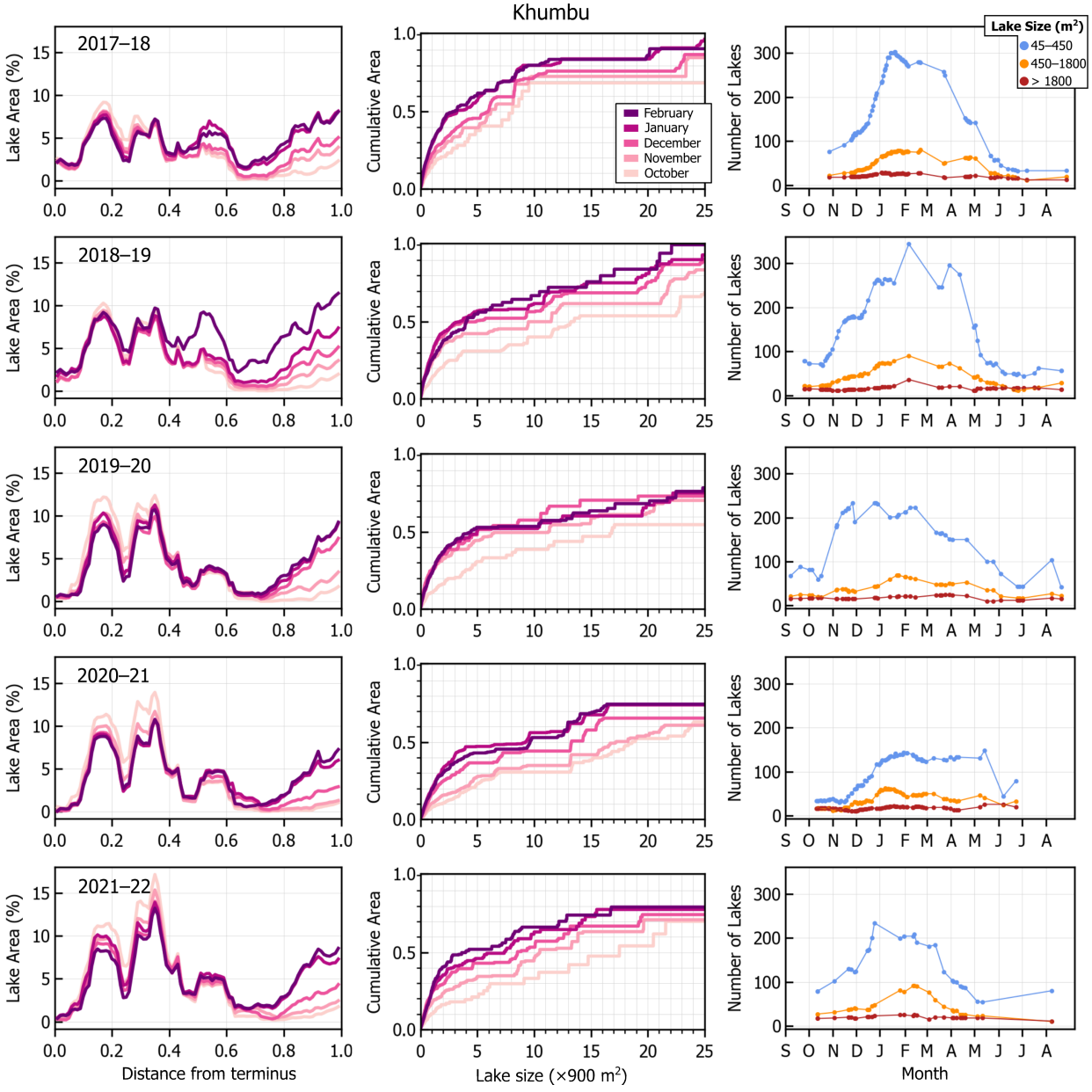

Figure S6. Seasonality in lake area and count on Khumbu Glacier, presented identically as Figure 10.

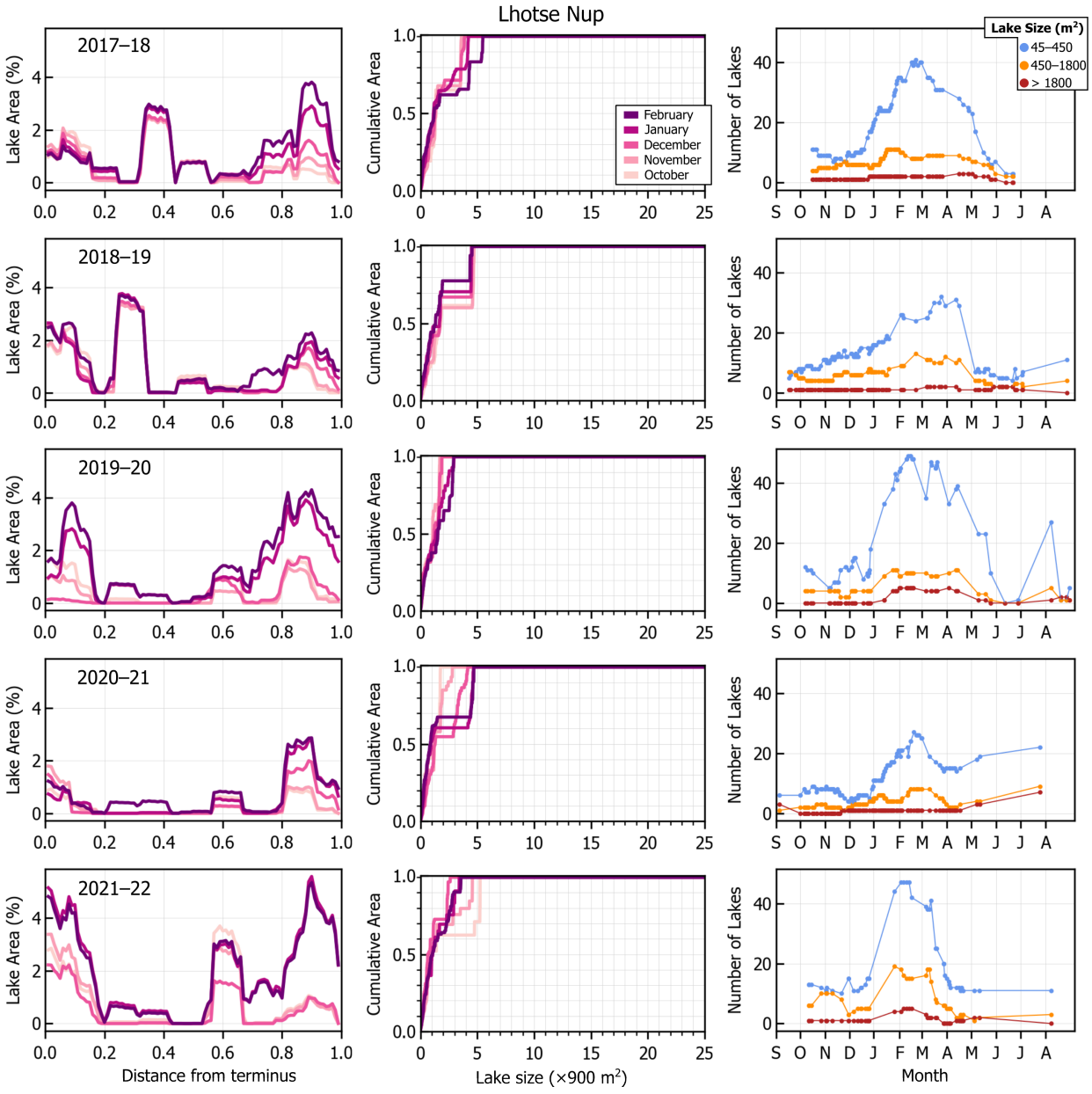

Figure S7. Seasonality in lake area and count on Lhotse Nup Glacier, presented identically as Figure 10.

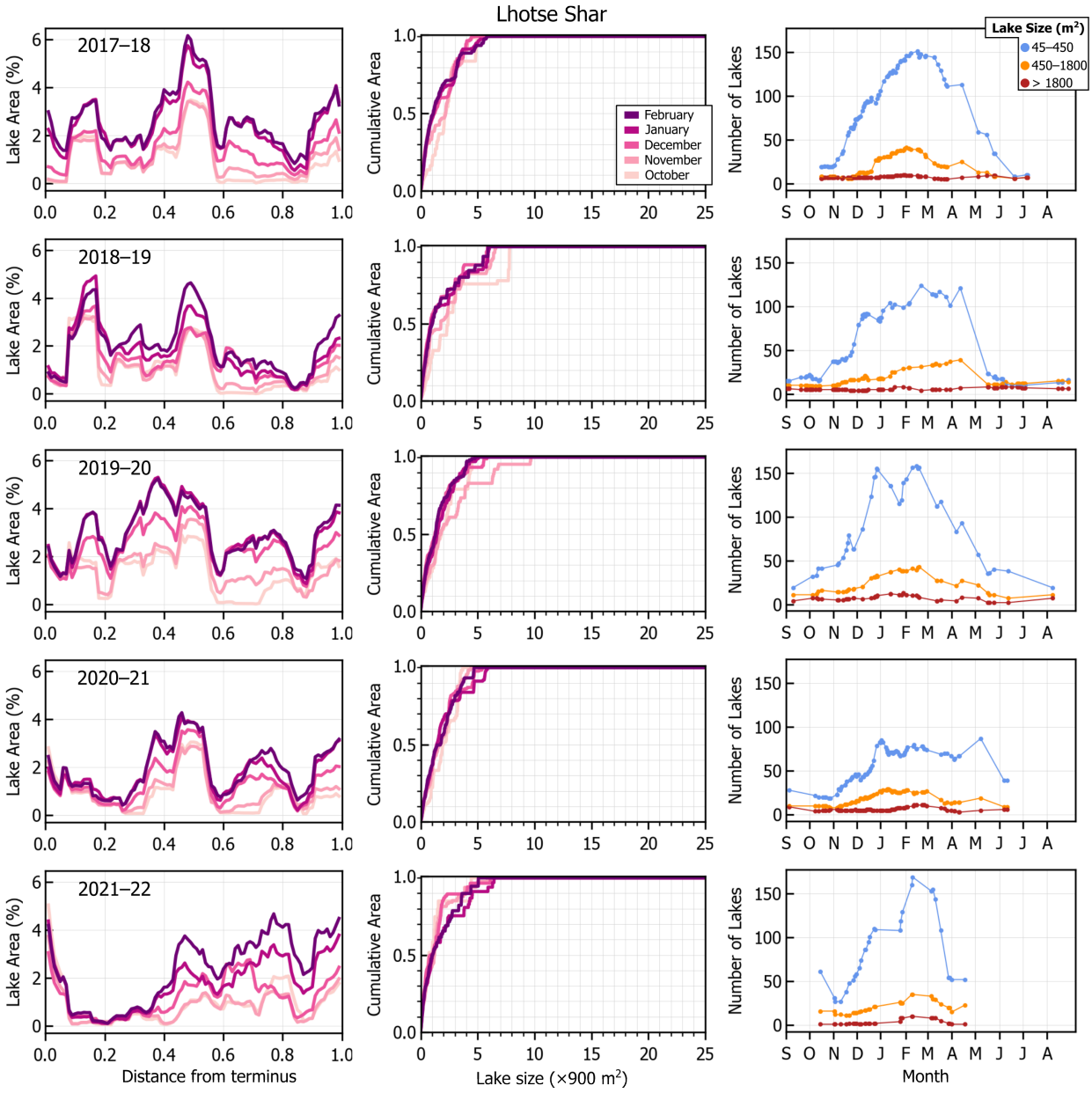

Figure S8. Seasonality in lake area and count on Lhotse Shar Glacier, presented identically as Figure 10.

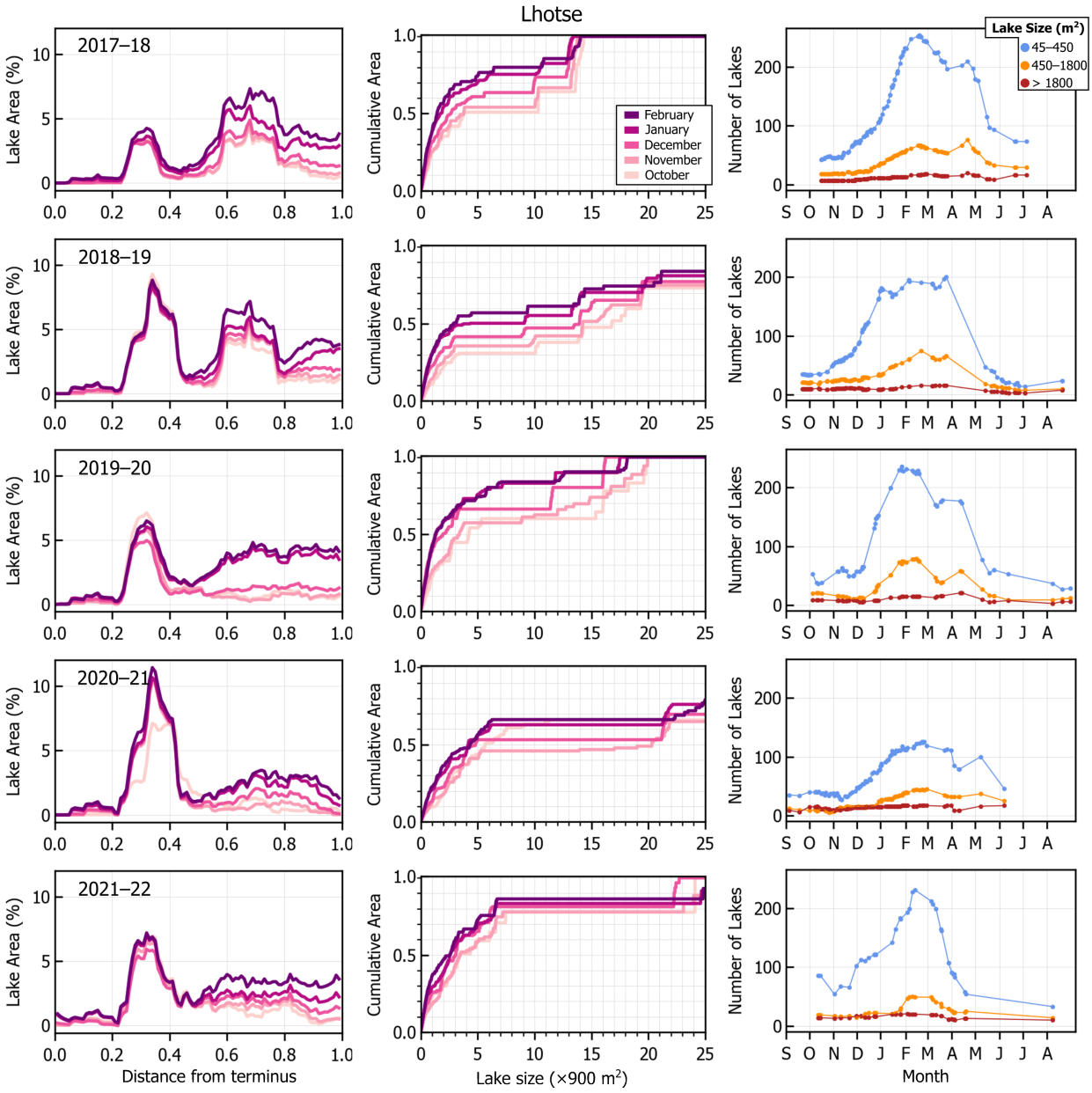

Figure S9. Seasonality in lake area and count on Lhotse Glacier, presented identically as Figure 10.

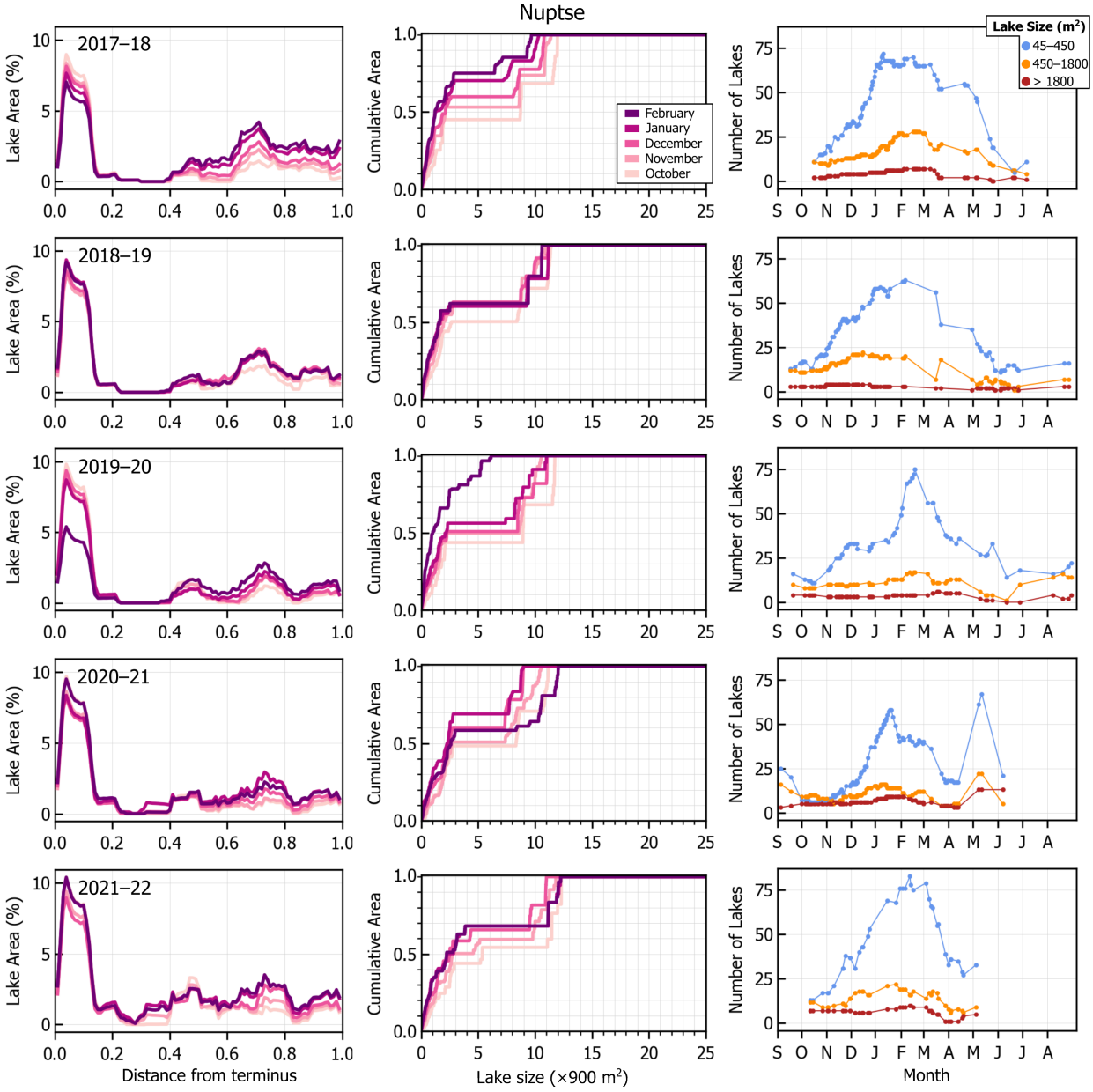

Figure S10. Seasonality in lake area and count on Nuptse Glacier, presented identically as Figure 10.

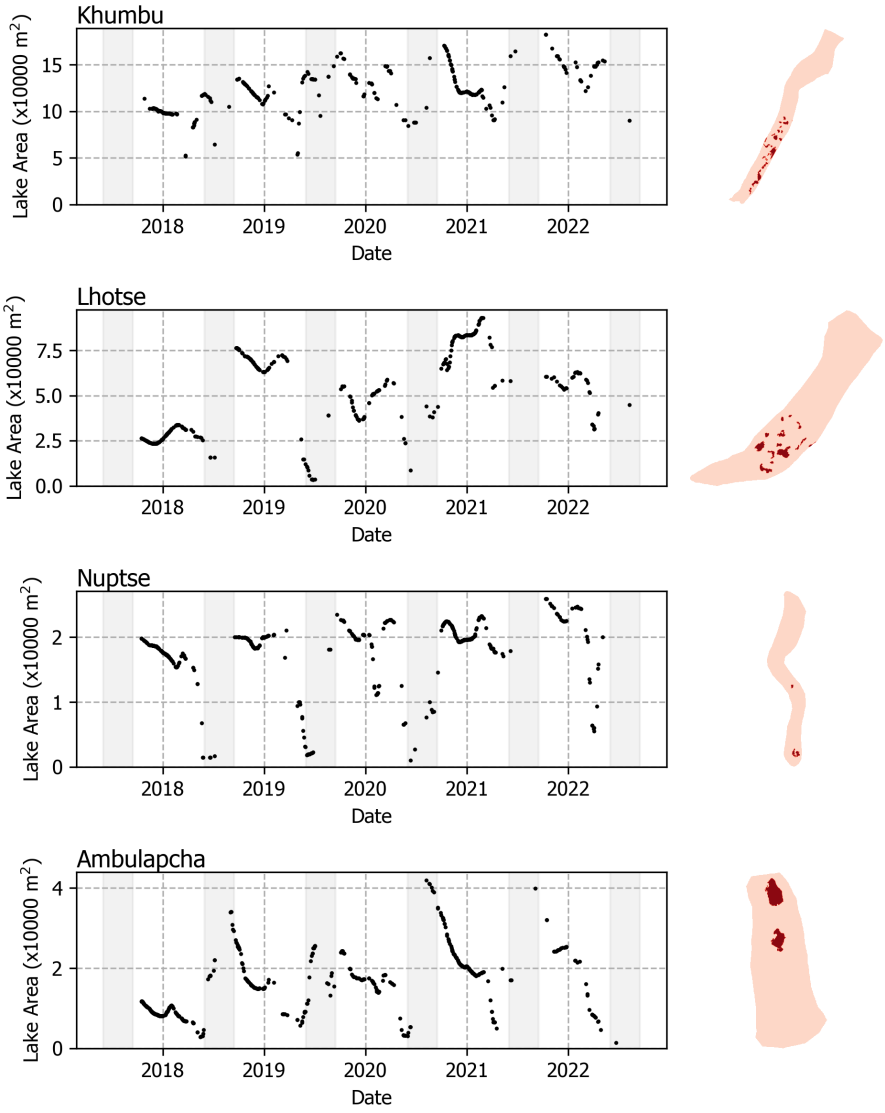

Figure S11. Seasonality of large, near-terminus lakes. Defined as lakes in the lower half of the debris covered area, with maximum extents greater than or equal to 3 Landsat pixels (2700 m^2)

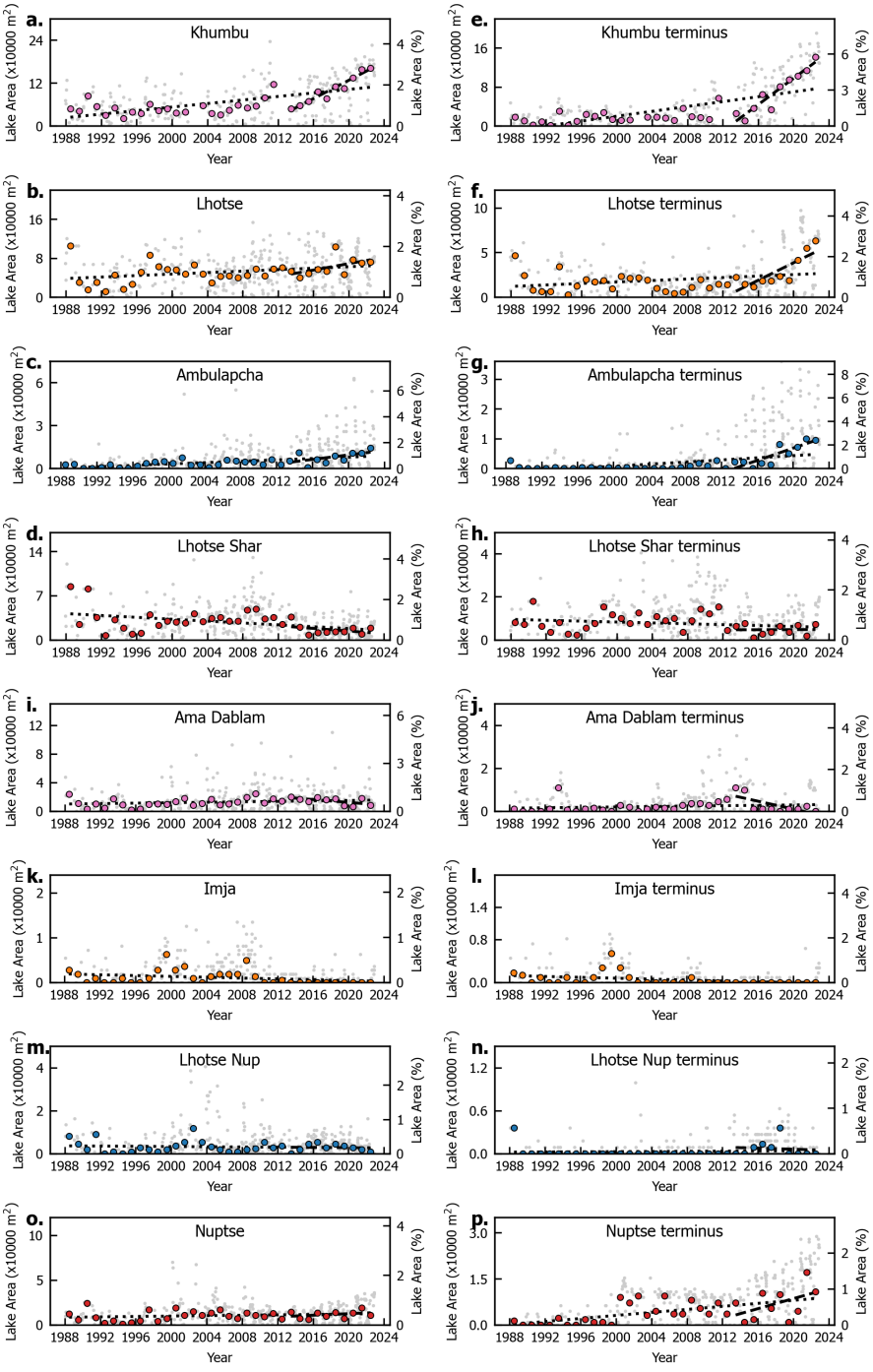

Figure S12. Landsat-derived time series of SGL area of all 8 glaciers.

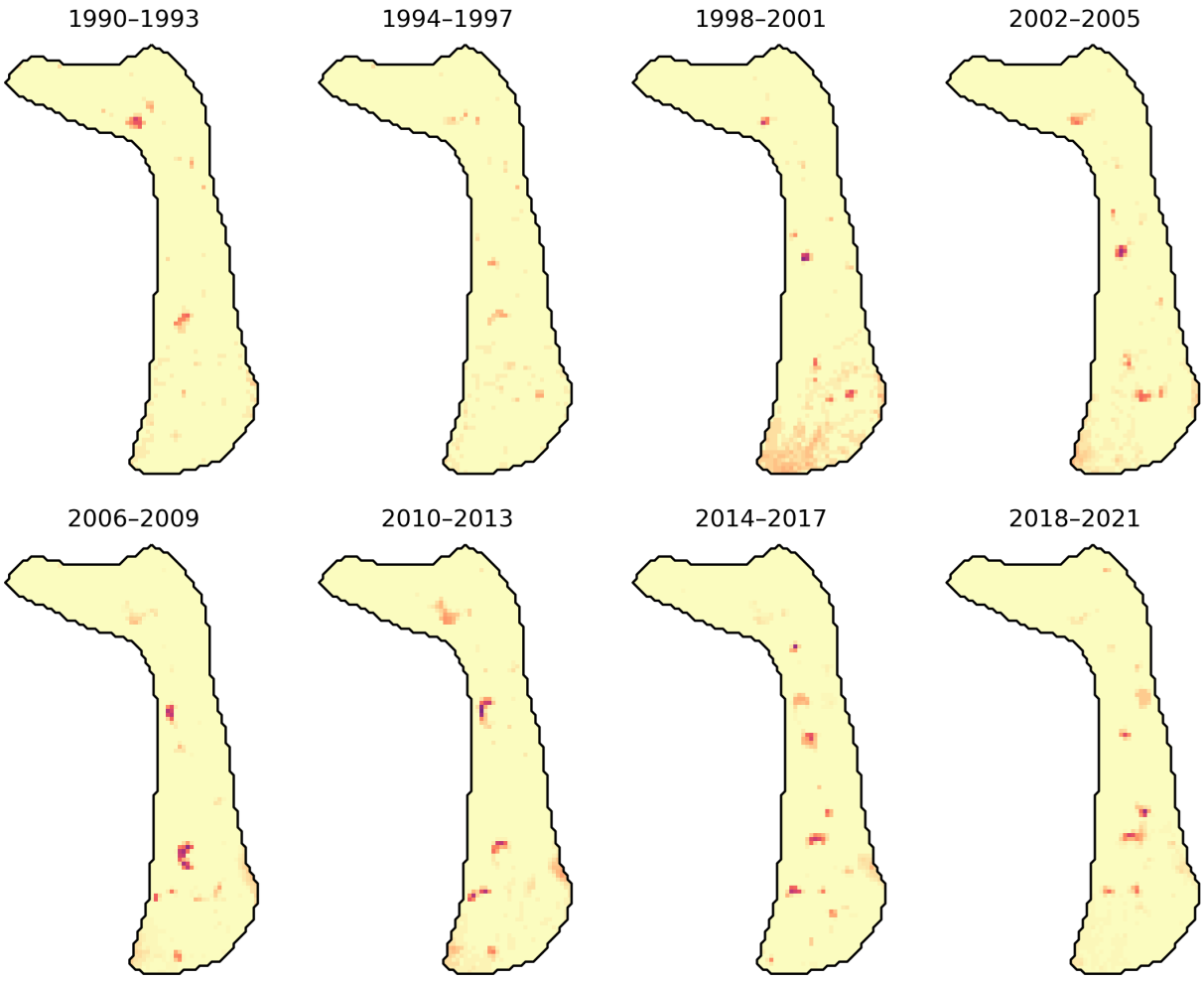

Figure S13. Repeat 4-year maps of SGLs on Ama Dablam Glacier, from Landsat imagery.

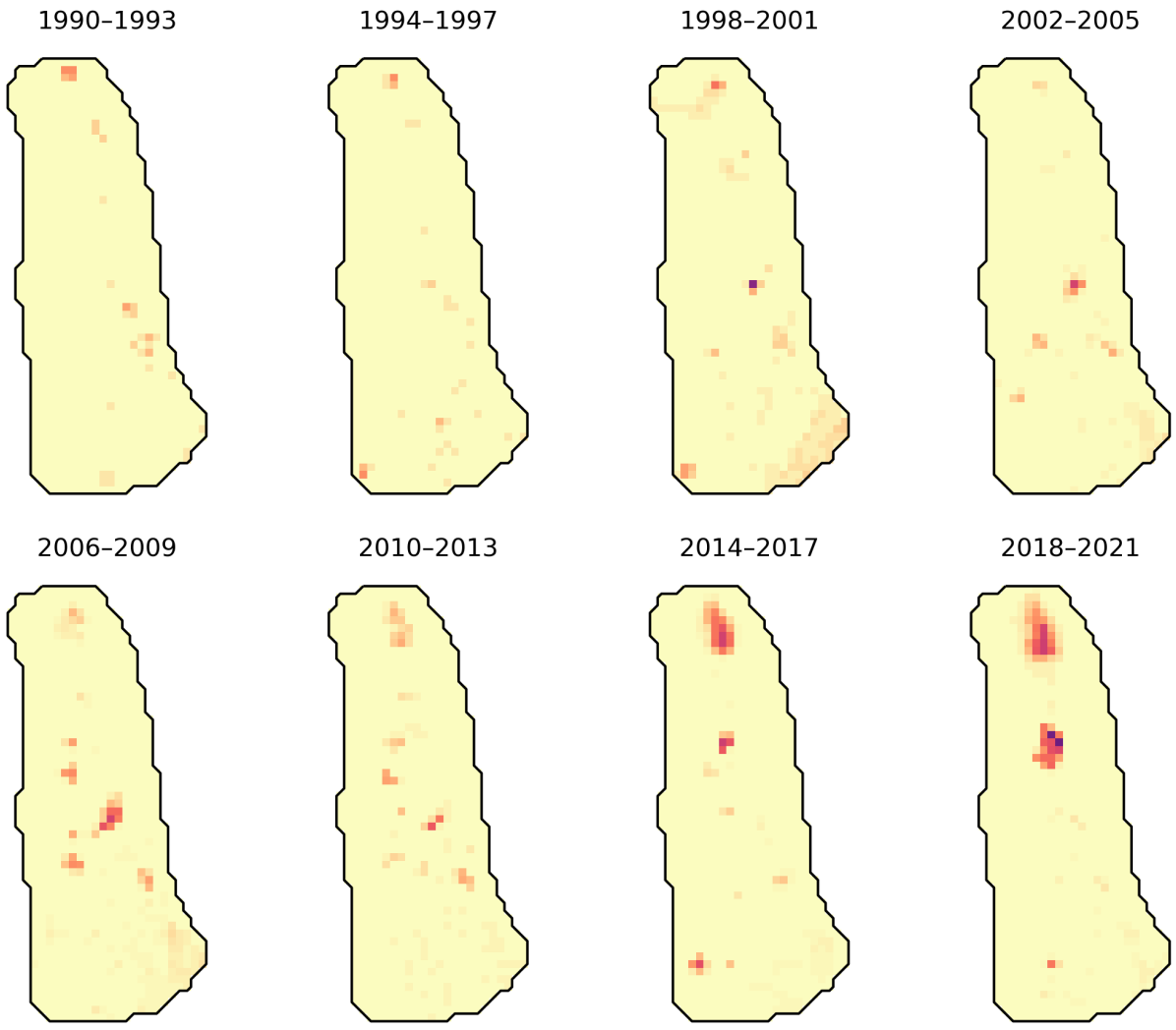

Figure S14. Repeat 4-year maps of SGLs on Ambulapcha Glacier, from Landsat imagery.

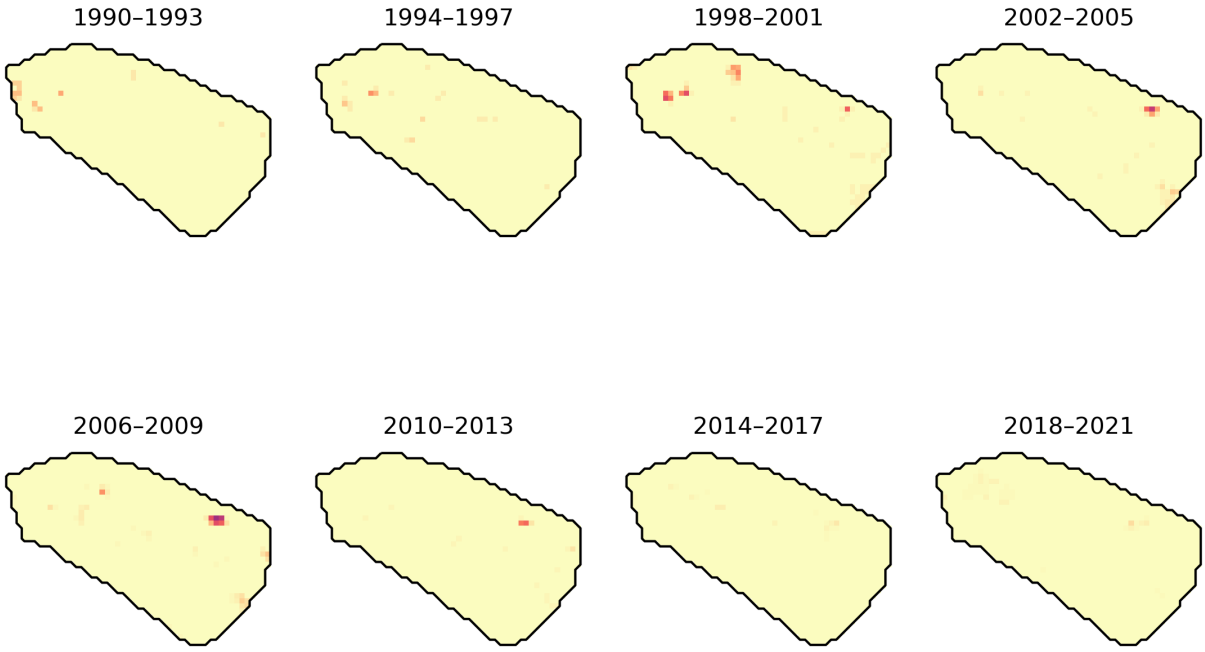

Figure S15. Repeat 4-year maps of SGLs on Imja Glacier, from Landsat imagery.

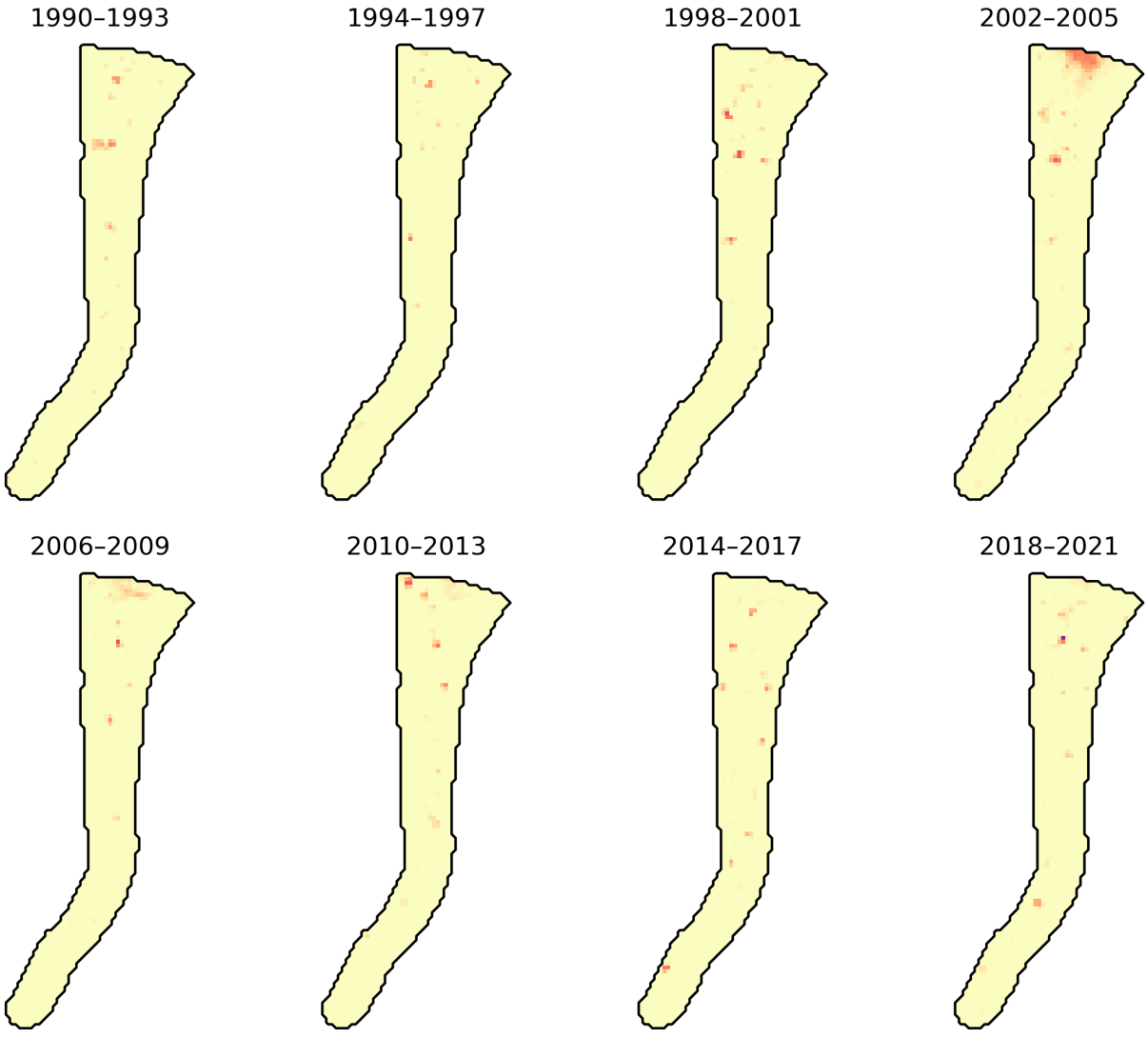

Figure S16. Repeat 4-year maps of SGLs on Lhotse Nup Glacier, from Landsat imagery.

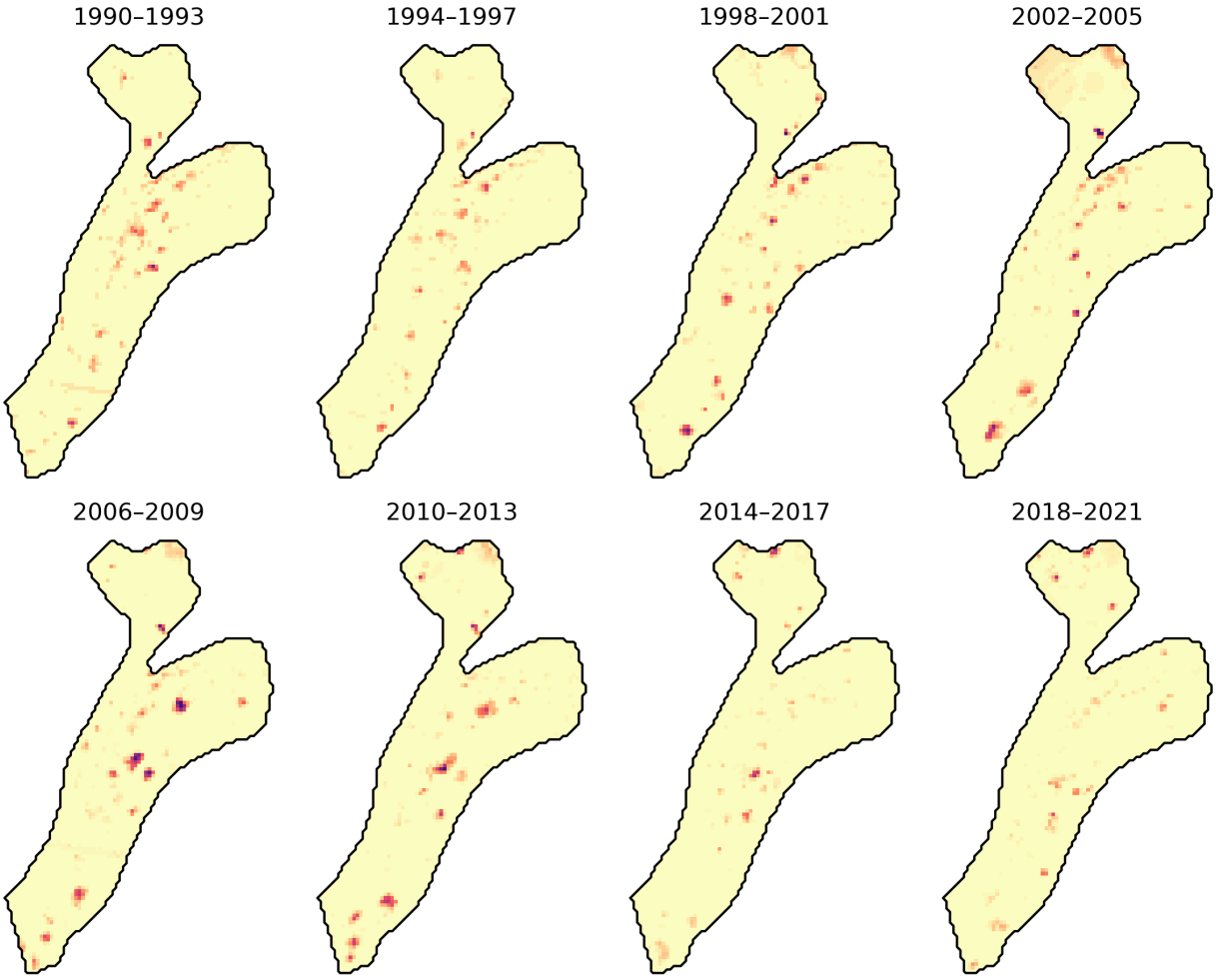

Figure S17. Repeat 4-year maps of SGLs on Lhotse Shar Glacier, from Landsat imagery.

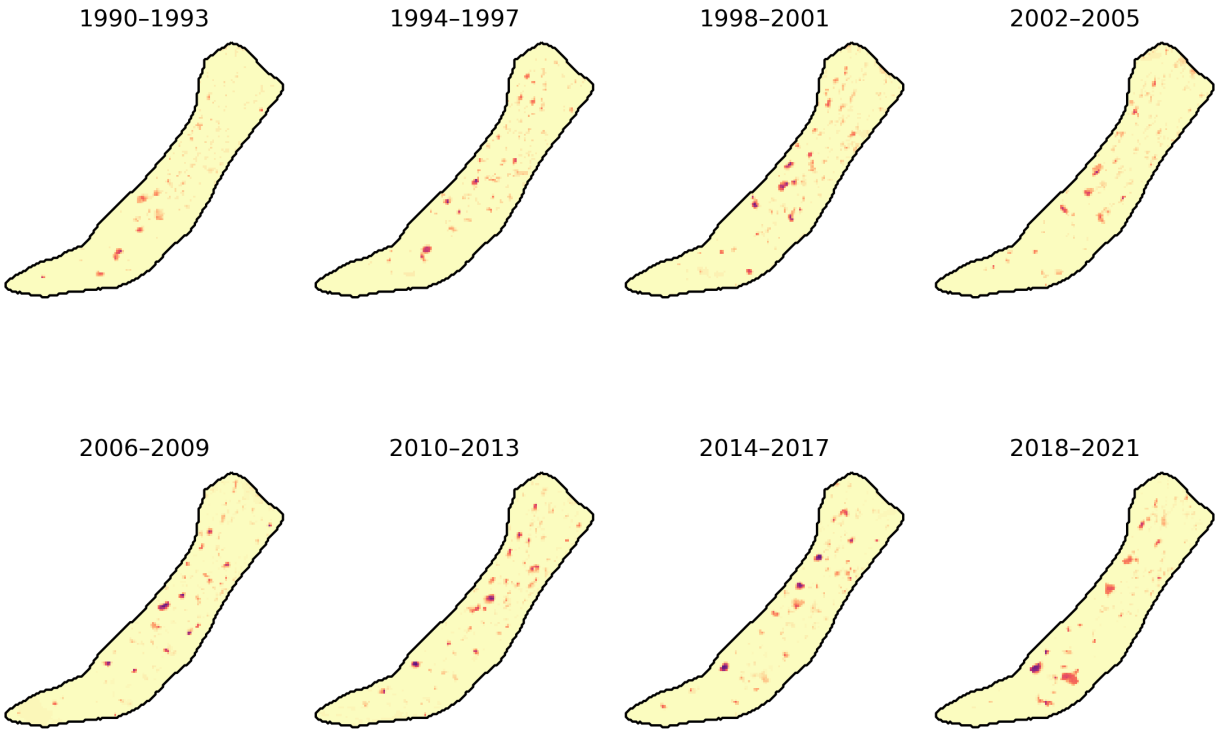

Figure S18. Repeat 4-year maps of SGLs on Lhotse Glacier, from Landsat imagery.

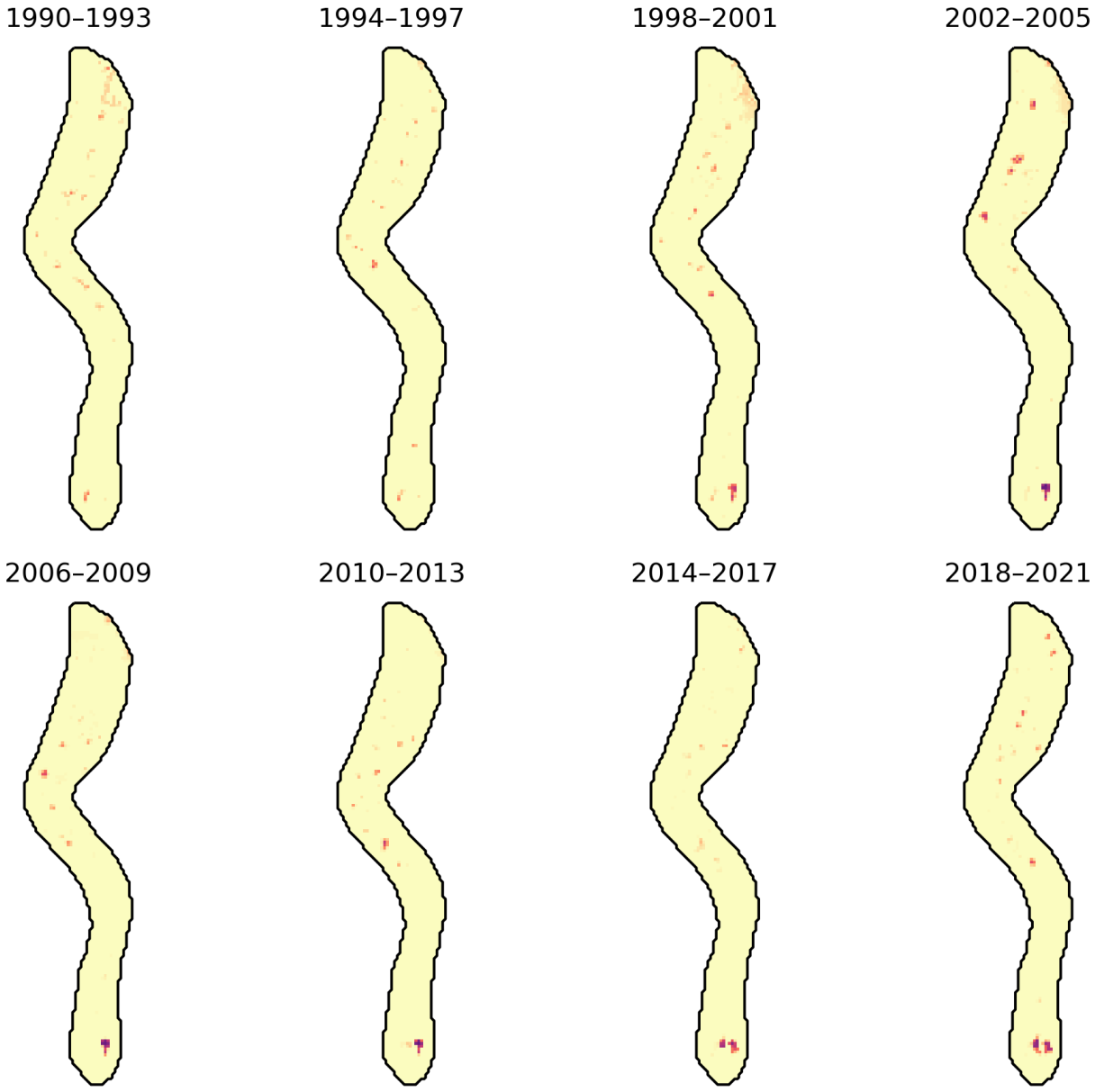

Figure S19. Repeat 4-year maps of SGLs on Nuptse Glacier, from Landsat imagery.